Acta Biomaterialia xxx (xxxx) xxx

Contents lists available at ScienceDirect

Acta Biomaterialia

journal homepage: www.elsevier.com/locate/actbio

Full length article

Targeting extracellular matrix glycation to attenuate fibroblast activation

Minjeong Jang[a,b], Seung Won Oh[a], Yunji Lee[a], Jin Young Kim[c], Eun Sun Ji[c], Pilnam Kim[a,d,*]

[a] Department of Bio and Brain Engineering, KAIST, Daejeon 34141, Republic of Korea
[b] Center for BioMicrosystems, Brain Science Institute, Korea Institute of Science and Technology (KIST), Seoul 02792, Republic of Korea
[c] Research Center for Bioconvergence Aanlysis, Korea Basic Science Institute, Ochang, Cheongju, 28119, Republic of Korea
[d] KAIST Institute for Health Science and Technology, Daejeon 34141, Republic of Korea

ARTICLE INFO

Article history:
Received 28 June 2021
Revised 14 January 2022
Accepted 18 January 2022
Available online xxx

Keywords:
Extracellular matrix (ECM)
Advanced Glycation End-products (AGEs)
Fibroblast activation
ECM-targeting

ABSTRACT

The extracellular matrix (ECM) of the tumor microenvironment undergoes constant remodeling that alters its biochemical and mechano-physical properties. Non-enzymatic glycation can induce the formation of advanced glycation end-products (AGEs), which may cause abnormal ECM turnover with excessively cross-linked collagen fibers. However, the subsequent effects of AGE-mediated matrix remodeling on the characteristics of stromal cells in tumor microenvironments remain unclear. Here, we demonstrate that AGEs accumulated in the ECM alter the fibroblast phenotype within a three-dimensional collagen matrix. Both the AGE interaction with its receptor (RAGE) and integrin-mediated mechanotransduction signaling were up-regulated in glycated collagen matrix, leading to fibroblast activation to acquire a cancer-associated fibroblast (CAF)-like phenotype. These effects were blocked with neutralizing antibodies against RAGE or the inhibition of focal adhesion (FA) signaling. An AGE cross-link breaker, phenyl-4,5-dimethylthiazolium bromide (ALT 711), also reduced the transformation of fibroblasts into the CAF-like phenotype because of its dual inhibitory role in the AGE-modified matrix. Apart from targeting the AGE–RAGE interaction directly, the decreased matrix stiffness attenuated fibroblast activation by inhibiting the downstream cellular response to matrix stiffness. Our results suggest that indirect/direct targeting of accumulated AGEs in the ECM has potential for targeting the tumor stroma to improve cancer therapy.

Statement of significance

Advanced glycated end-products (AGEs)-modified extracellular matrix (ECM) is closely associated with pathological states and is recognized as a critical factor that precedes tumorigenesis. While increased matrix stiffness is known to induce fibroblast activation, less is known about how both biochemical and mechano-physical changes in AGE-mediated matrix-remodeling cooperate to produce a myofibroblastic cancer-associated fibroblast (CAF)-like phenotype. For the first time, we found that both the AGE interaction with its receptor (RAGE) and integrin-mediated mechanotransduction were up-regulated in glycated collagen matrix, leading to fibroblast activation. We further demonstrated that an AGE cross-link breaker, ALT-711, reduced the CAF-like transformation because of its dual inhibitory role in the AGE-modified matrix. Our findings offer promising extracellular-reversion strategies targeting the non-enzymatic ECM glycation, to regulate fibroblast activation.

1. Introduction

In the tumor microenvironment, abnormal extracellular matrix (ECM) remodeling is accompanied by tumor malignancy and metastatic progression due to the disrupted balance between ECM synthesis and degradation and the altered expression of matrix-remodeling enzymes [1]. One of the factors resulting in ECM remodeling is non-enzymatic glycation, a spontaneous reaction between reducing sugars and polypeptides that ultimately leads to the accumulation of advanced glycation end products (AGEs) within the matrix [2–6].

Hyperglycemia is recognized as a general risk factor for cancer development and is associated with cancer malignancy [7]. In hyperglycemic microenvironments, AGEs accumulate spontaneously within the ECM, which ultimately increases the stiff-

* Corresponding author.
E-mail address: pkim@kaist.ac.kr (P. Kim).

https://doi.org/10.1016/j.actbio.2022.01.040
1742-7061/

ness of collagen fibrils and modifies their architecture [4,8,9]. Abnormally aligned, straight, thickened collagen fibers are characteristic of desmoplastic tumor stroma [10–12], and these matrix changes alter cell–matrix interactions and transform cellular phenotypes. Receptors of AGE (RAGE) interact with AGEs, and such AGE-RAGE interactions are well-known to activate several signaling pathways, such as nuclear factor kappa-light chain enhancer of activated B cells (NF-κB), extracellular signal regulated kinase (ERK), or phosphoinositol-3-kinase (PI3K), inducing several cellular responses, such as apoptosis, production of pro-inflammatory cytokines, and reactive oxygen species (ROS) [9]. However, the pathogenic link underlying the AGE-mediated matrix and the development of pro-tumorigenic stroma has not been fully elucidated. Fibroblasts are common stromal cells in tissues [13] and constitute up to 80% of a tumor [14]. In addition, fibroblasts are highly sensitive to extra- and intercellular signaling, which allows these cells to actively remodel their ECM and trigger surrounding normal fibroblasts to transform into cancer-associated fibroblasts. While increased matrix stiffness is known to induce fibroblast activation [15–19], less is known about how both biochemical and mechano-physical changes in AGE-mediated matrix-remodeling processes cooperate to produce a myofibroblastic cancer-associated fibroblast (CAF)-like phenotype.

We investigated the effects of AGE-mediated matrix remodeling on fibroblast phenotype by studying cells cultured within pre-glycated collagen matrices, and found that targeting AGEs could attenuate the CAF-like transformation of fibroblasts, which is a potential therapeutic application to modulate the tumor microenvironment.

2. Materials and methods section

2.1. Development of pre-glycated 3D matrix

To pre-glycate collagen, collagen (Corning) was mixed with D-ribose (Sigma) in 0.1% acetic acid (Sigma) to achieve final concentrations of 0- and 500-mM ribose and incubated at 4 °C for 1 month. Then, the ribose-reacted collagen solution was neutralized with 10X DPBS (Welgene) and 1 M NaOH (Sigma) to form 4 mg/ml gels. The neutralized collagen solution was incubated at 37 °C for 1 hour to allow collagen to crosslink and form fibrils.

2.2. Human fibroblast cell culture

Human immortalized fibroblast cell line (hTERT NOF) was provided by Prof. Jae Ho Kim from Busan National University. Cells were cultured and maintained with DMEM/F12 (3:1 mixture, Welgene, Korea), supplemented by 1% penicillin/streptomycin (P/S, Welgene) and 10% fetal bovine serum (FBS, Welgene), in a humidified incubator at 37 °C and 5% CO_2. Culture medium was replaced every 2∼3 days and subcultured with 0.25% trypsin/EDTA (Welgene). For 3D cell culture in collagen and glycated collagen matrices, collagen solution was neutralized with 10X DPBS and 1 N NaOH and carefully mixed with fibroblast cells (5×10^5 cells per ml). Cell embedded collagen solution was polymerized at 37 °C for 1 hour, which was then maintained for the duration of the experiment.

2.3. Construction of RAGE-depleted fibroblasts

RAGE shRNA (Santa Cruz, sc-36374-sh) were used to generate RAGE-depleted hTERT NOF cells by following the manufacturer's protocol. Briefly, 1 µg of shRNA and 5 µl of shRNA Plasmid Transfection Reagent (Santa Cruz, sc-108061) were diluted in Plasmid Transfection Medium (Santa Cruz, sc-108062). shRNA mixtures were gently added into cell cultured well and incubated for 12 h at 37 °C. Following incubation, the medium was replaced, and the cells were incubated for an additional 24–48 h. To select RAGE-depleted cells, 5 µg/ml of puromycin dihydrochloride (Invivogen, ant-pr-1) were used.

2.4. AGE-BSA solution treatment

AGE-BSA was prepared by incubating BSA (0.5% bovine serum albumin, Sigma) and D-ribose (250 mM, Sigma) in DPBS (Lonza) at 4 °C for over one month. BSA solution without ribose was used as a control. AGE-BSA and BSA solutions were mixed at a 1:10 ratio with culture media and used to culture fibroblasts in a non-glycated collagen matrix for 7 days, and AGE-BSA and BSA-containing-culture media were changed every 2∼3 days.

2.5. Analysis of mechanical properties

Glycated and non-glycated matrix samples were mechanically characterized by determining the storage (G′) and loss (G″) moduli with a Rheometer (MCR92, Anton Paar). Samples were loaded between a parallel plate measuring detector with a diameter of 8 mm and measured with the frequency sweep mode at constant strain (1%). The storage modulus was calculated at 1 Hz.

2.6. Mass spectroscopy

Trypsin Digestion: Glycated and non-glycated collagen matrix with 0- and 500 mM D-ribose were prepared to analyze AGE or its derivative by using mass spectrometry. The proteins in collagen matrix were reduced with DTT (Sigma) at 60 °C for 60 min and then alkylated with IAA (Sigma) for 45 min in the dark. Then, the alkylation was quenched with DTT. The proteins in collagen matrix were digested with trypsin (1:20 of enzyme to protein ratio) in 50 mM NH_4HCO_3 (Sigma) at 37 °C for 16 h. Tryptic peptides were desalted using solid phase extraction (SPE) on a Bravo platform (Agilent, USA) and then dried under vacuum.

Liquid chromatography-mass spectrometry: Dried samples were reconstituted in 50ul of 0.1% formic acid (Sigma) in DW and analyzed using a LC-MS/MS system consisting of an EASY-nanoLC System (Thermo Scientific, USA) and an Orbitrap Fusion Lumos mass spectrometer (Thermo Scientific, USA) equipped with an EASY-Spray™ source. The peptides were loaded into Acclaim PepMap™ 100 (75um x 2 cm, nanoViper) for 4 min at a flow rate of 4 μL/min. Then, the peptides were separated on a PepMap™ RSLC column (C_{18} particle size 2 μm, 100A, 75 μm x 50 cm). The mobile phases, A and B, were composed of 0 and 80% acetonitrile (B&J), respectively, and each contained 0.1% formic acid. The LC gradient began with 2% B and was ramped to 5% B over 1 min, to 10% B over 16 min, to 50% B over 74 min, to 100% B over 1 min, and remained at 100% B over 8 min and 2% B for another 5 min. The column was re-equilibrated with 2% B for 15 min before the next run. The voltage applied to produce an electrospray was 1.9 kV. The scan range for MS spectrum was *m/z* 400–1600 with a resolution of 120,000. The maximum ion accumulation time was 50 ms. The AGC target was set to 400,000. The fragmentation by higher energy collisional dissociation (HCD) were acquired on a data-dependent using Top Speed mode with 3 s cycle time at a resolution 30,000. The intensity threshold was set to 5000. The maximum ion accumulation time was 54 ms. The AGC target was set to 50,000. The isolation window was 1.2 *m/z*. The normalized collision energy (NCE) was 27%. Dynamic exclusion was enabled for a duration of 12 s.

Data analysis: The LC-MS/MS date were analyzed by using SEQUEST HT in Proteome Discoverer software (Thermo Fisher Scientific, version 2.2) with UniProt human. Precursor and fragment mass tolerance were 10 ppm and 0.02 Da, respectively. Trypsin was selected as the specific proteolytic enzyme. Up to 2 missed

cleavage per peptide allowed for the search. Caramidomethylation of cysteine was set as a fixed modification. N-acetylation (protein N-terminal), oxidation (methionine), amadori-modified lysine/arginine, carboxymethyl lysine/arginine and carboxyethyl lysine/arginine, Argpyrimidine (arginine) and Methylglyoxal-derived hydroimidazolone (arginine) were set as variable modifications. Peptide and protein identifications were filtered at a false discovery rate (FDR) of 1%. All glycated peptide spectrum matches were examined manually.

2.7. Analysis of fibril structure

Confocal Microscopy: Col-F Collagen Binding Reagent (Immuno-Chemistry Technologies) was used to stain the fibril structure of collagen. Col-F was mixed at a 200:1 ratio (Collagen solution: Col-F) when the collagen solution was generated. After gelation, Col-F-conjugated collagen matrices were washed with DPBS (Welgene) three times and were imaged using a confocal microscope (Nikon).

Scanning electron microscopy (SEM): The fibrillar structure of collagen was imaged through Field Emission Scanning Electron Microscopy (Magellan400, FEI, USA). Glycated and non-glycated collagen matrices were stored in DPBS and dehydrated by gradually increasing the ethanol concentration in the storing buffer from 50 to 100% ethanol, for 5 min each. Samples were then air-dried in a fume hood for 1 day. Dehydrated samples were mounted with double-sided carbon tape and sputter coated with platinum (Pt) before SEM imaging.

2.8. Gene ontology (GO) analysis

The online-accessible Gene Expression Omnibus (GEO) database (GSE22862, 15 primary non-small cell lung carcinoma (NSCLC) fibroblasts (CAF) and 15 matched normal lung fibroblasts (NF)) were used to analyze enriched GO terms. Genes were ranked by fold changes (FC), and up-regulated 444 genes (FC[CAF/NF]>0, $p<0.05$) were used to analyze GO term enrichment. Gene Ontology (GO) term enrichment to classify Kyoto Encyclopedia of Genes and Genomes (KEGG) pathway by using EnrichR program (http://amp.pharm.mssm.edu/Enrichr/) ranked by p-value.

2.9. Antibodies and inhibitors

Integrin ß1, FAK, pFAK^{Y397}, AGE antibodies were purchased from Abcam. Antibodies against RAGE, YAP, GAPDH, Lamin A/C, ß-tubulin were purchased from Santa Cruz. FAP (Bioss), α-SMA (eBioscience), fibronectin (Santa Cruz), and vimentin (Cell signaling) antibodies were used to analyze CAF-like transition. TRITC-Phalloidin and 4,6-diamidino-2-phenylindole (DAPI) were purchased from Sigma-Aldrich to stain F-actin and the nucleus, respectively. FPS-ZM1 (Abcam), Y15 (Sigma), and ALT-711 (KareBay Chem) were prepared following the manufacturer's manual and stored at −20 °C.

2.10. WST-8 assay

To analyze fibroblast survival and proliferation in each condition, WST-8 assays (Quanti-MAX^{TM} WST-8 Cell Viability Assay Kit, BIOMAX) were performed according to the manufacturer's manual. Absorbance was measured by SpectraMax iD3 Multimode Microplate Reader (Molecular Devices) at 450 nm after reaction.

2.11. Analysis of reactive oxygen species (ROS)

Reactive oxygen species (ROS) were detected by using DCFDA/H2DCFDA-cellular reactive oxygen species detection assay kit (Abcam) according to the manufacturer's manual. 2′,7′-Dichlorofluorescein (DCF), which is the reaction product of ROS and DCFDA, was observed by using confocal microscopy (Carl Zeiss LSM700, ex./em. at 485 nm/535 nm).

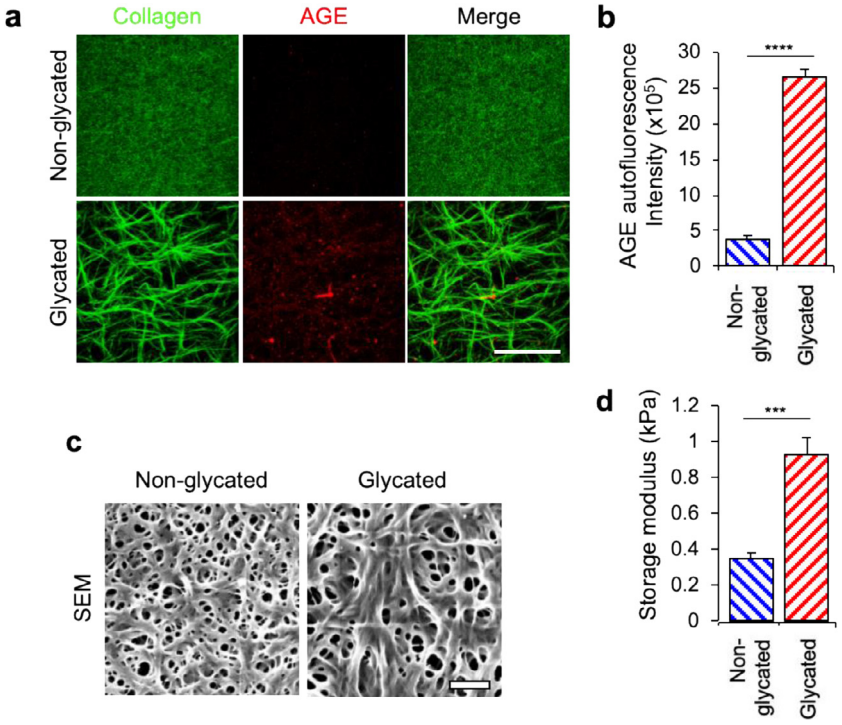

Fig. 1. Characterization of the glycated collagen matrix. (a) Immunostaining images of glycated collagen shows that AGEs observed in 500 mM glycated matrix. Green: collagen fiber stained by Col-F, red: AGE. Scale bar = 50 μm (b) Autofluorescence intensity of AGEs (Ex370/Em440). ****;$p<0.0001$ (c) SEM images were obtained from non-glycated and glycated collagen with 0, 500 mM ribose concentration to confirm the collagen fibril structure. Scale bar = 1 μm (d) The storage modulus of non-glycated and glycated collagen was measured by rheological study ($n = 8$). ***; $p<0.001$. (For interpretation of the references to colour in this figure legend, the reader is referred to the web version of this article.)

2.12. Immunofluorescent staining

Fibroblasts in collagen matrices were fixed with 4% paraformaldehyde (Biosesang, Korea), permeabilized with 0.15% Triton X-100 (Sigma), and blocked with 1 wt% BSA (Sigma). Samples were incubated with primary antibodies overnight at 4 °C. Subsequently, samples were incubated with FITC or TRITC-conjugated secondary antibodies (1:1000; Sigma). F-actin was stained with TRITC-phalloidin. All immunostaining images were counterstained with DAPI for the nucleus. Fluorescence images were captured with confocal microscopy (Nikon).

2.13. Gene expression analysis

For analysis of mRNA expression, total RNA of fibroblasts within the glycated matrix was extracted by using the phenol/chloroform method. Fibroblasts from glycated matrices were crushed and homogenized by a disposable hand-held homogenizer with Trizol reagent (Ambion). After homogenization, the aqueous RNA phase was separated by adding chloroform, collected, and precipitated by isopropyl alcohol and glycogen. Precipitated RNA pellets were washed by 70% ethanol in diethyl pyrocarbonate (DEPC) water. After dehydration of RNA pellets, RNA samples were dissolved in DEPC water (Biosesang). The quantity and purity of the extracted total RNA were measured using spectrophotometry (DeNovix), and reverse-transcribed to cDNA by using the iScript cDNA synthesis kit (BioRad). RT-qPCR was performed in a thermal cycler (BioRad) using a SYBR Green Real-time PCR Master Mix (Toyobo, Osaka, Japan). Analyses of relative mRNA expressions were normalized by GAPDH, a house-keeping gene. All primer sequences are summarized in Supplementary Table S2. Gene expression data from RT-PCR were visualized by heatmap analysis based on the z-score. z-score were calculated for every row by formula; z-score = (relative mRNA expression values - mean)/standard deviation. And each z-scores were visualized by heatmap of Prism ver 8 (GraphPad) software. Red and blue indicates over- and under-expression of genes, respectively.

2.14. Protein expression analysis

Proteins in fibroblasts from collagen matrices were extracted using RIPA buffer (1X, Sigma-Aldrich) supplemented with Halt™ Protease and Phosphatase Inhibitor Cocktail (Thermo Scientific). Cytoplasm and nuclear proteins were extracted separately using NE-PER Nuclear and Cytoplasmic Extraction Reagents (Thermo Scientific) following the manufacturer's protocol. The concentrations of extracted proteins were measured by Bradford assays (BioRad). 20 μg of protein were loaded onto each well of SDS-PAGE gels, then transferred to nitrocellulose membrane (Amersham) for blotting. Primary antibodies and HRP-conjugated secondary antibodies were added to label target proteins. Protein expression was detected by using Pierce ECL western blotting substrate (Thermo Scientific), and membranes were imaged using a membrane imaging system (ImageQuant LAS 4000 mini, GE Healthcare).

2.15. Statistical analysis

All experiments were held in triplicate, at a minimum, and individual experiments were normalized to control values and expressed as mean ± standard deviation. Two-tailed Student's t-tests were utilized to determine statistical significance. p-values are represented as asterisks (*) on graphs; *; $p<0.05$, **; $p<0.01$, and ***; $p<0.001$.

3. Results and discussion

3.1. Confirmation of an AGE-modified collagen matrix

We constructed a glycated collagen matrix that simulates the in vivo glycation of matrix characterized by biochemically generated

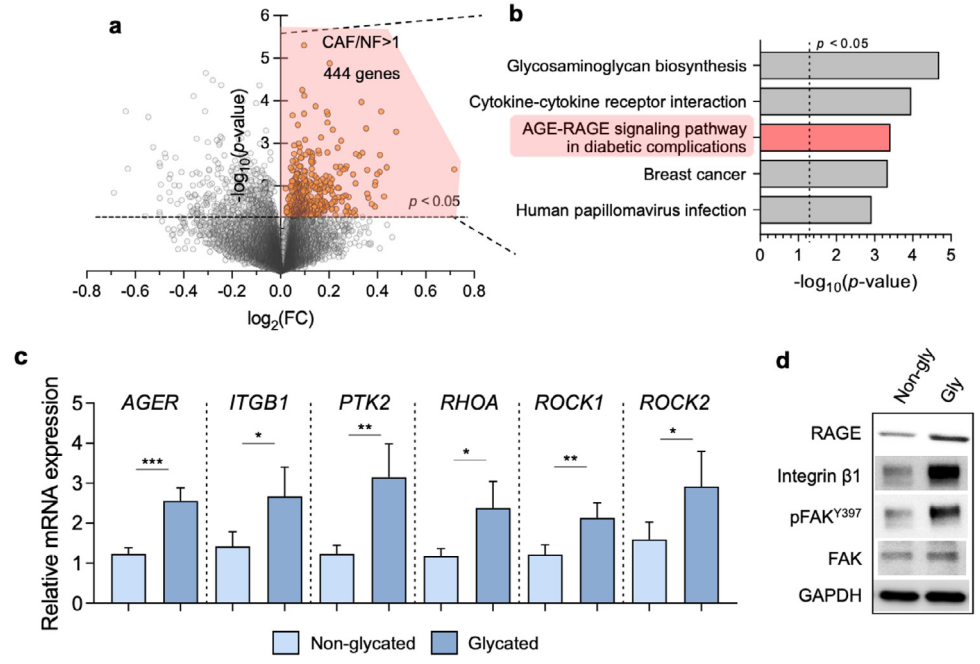

Fig. 2. Change of AGE-RAGE and mechanotransduction signaling by collagen glycation. (a) Volcano plot showing statistical significance (p-value) versus fold change (FC) of CAFs and NFs (GSE22862, 15 primary non-small cell lung carcinoma (NSCLC) fibroblast and 15 matched normal lung fibroblasts). 444 up-regulated genes (orange points) were used to analyze GO term enrichment. (b) Gene ontology (GO) analysis of significantly up-regulated 444 genes in CAF ($p<0.05$, FC(CAF/NF)>1). (c) The relative mRNA expression of AGER, ITGB1, PTK2, RHOA, and ROCK1/2 in non-glycated and glycated matrix *;$p<0.05$, **;$p<0.01$, and ***;$p<0.001$ (d) Total RAGE, integrin $\beta 1$, pFAK^{Y397}, FAK protein expression in non-glycated and glycated matrix. Loading control is GAPDH.

AGE formation, or glycation, and increased stiffness with dysregulated ECM structure. A collagen solution was pre-glycated with D-ribose dissolved in 0.1% acetic acid at 4 °C; ribose was selected due to its faster kinetics compared to other reducing sugars [20]. Ribose reacts with lysine and arginine sites in collagen chains and is transformed into argpyrimidine or carboxymethyl (CM), which are the main AGE molecules [21]. The Maillard reaction induces collagen crosslinking via AGE generation [22,23]. Using tandem mass spectroscopy, we confirmed AGE formation in glycated collagen by analyzing the amount of CM in lysine and arginine (Supplementary Figure S1, Table S1), which are common sites for AGE formation [24]. The CM levels at specific sites of the collagen alpha-I chain increased under glycated conditions (ribose 500 mM), compared to the non-glycated condition. In addition, we observed thick, linearized collagen fibers in glycated matrix (collagen, green; AGE, red; Fig. 1a) through immunofluorescence microscopy. We measured the autofluorescence of AGEs (excitation, 370 nm; emission, 440 nm) and observed a ~3.5-fold increase in the glycated matrix compared to the non-glycated matrix (Fig. 1a, b).

Next, we examined the changes in the mechanical and structural properties of the glycated matrix. Due to the excessive crosslinking of collagen fibers, the bulk storage modulus of the glycated collagen was significantly elevated compared to the non-glycated matrix, even at the same collagen concentration of 4 mg/mL (Fig. 1d). Scanning electron microscopy images revealed a thick fibrous structure due to abnormal collagen crosslinking in the glycated matrix (Fig. 1c). Therefore, we confirmed that a non-enzymatic glycated collagen matrix had been fabricated successfully, with linearized, stiffened, and highly crosslinked collagen fibers observed in the tumor microenvironment [6].

3.2. The glycated matrix induces both RAGE expression and mechanotransduction signaling

Given that AGEs exert effects both directly through the formation of collagen cross-links that alter the mechanical properties of ECM [25] and by interacting with specific cell surface receptors, we examined the mechanisms through which AGEs contribute to cellular signaling pathways: (1) the most prominent AGE-mediated signaling cascades via the AGE receptor (RAGE; receptor of advanced glycation end-products) interactions on the cell surface and (2) mechanotransduction via ECM–integrin interactions. As biomechanical sensors, integrins mediate cell adhesion and transmit mechanical cues to the cells [26].

To examine the mechanism based on RAGE ligand-mediated fibroblast activation, we first identified gene sets that were significantly enriched in CAFs compared to normal fibroblasts (NFs) using the online-accessible Gene Expression Omnibus database (GSE22862, 15 primary non-small cell lung carcinoma (NSCLC) fibroblasts and 15 matched normal lung fibroblasts) (Fig. 2a).

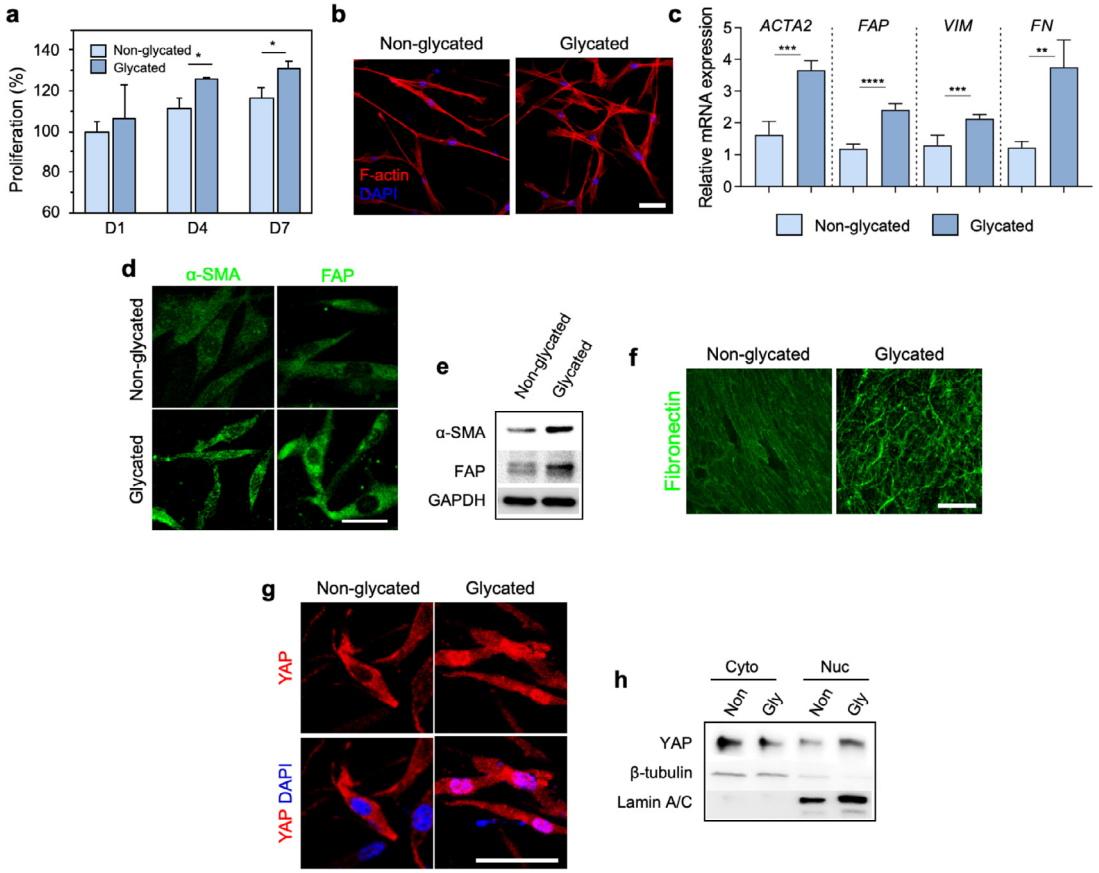

Fig. 3. Analysis of fibroblast activation in glycated matrix. (a) Cell viability in day 1, 4, and 7 in the non-glycated and glycated matrix. *;$p<0.05$ (b) Immunofluorescence staining of F-actin (red) in the glycated matrix. Nucleus (blue) were counter-stained by DAPI. Scale bar = 50 μm (c) The relative mRNA expression of ACTA2 (α-SMA), FAP (FAP), VIM (vimentin) and FN (fibronectin) in non-glycated and glycated matrix. Gene expression normalized by GAPDH. **;$p<0.01$, ***;$p<0.001$, ****;$p<0.0001$. (d) Immunofluorescence staining of α-SMA (green) and FAP (green) of fibroblast cultured in the glycated matrix. Nucleus (blue) were counter-stained by DAPI. Scale bars= 50 μm (e) Total α-SMA and FAP protein expression in non-glycated and glycated matrix. Band intensity normalized by GAPDH. (f) Expression of fibronectin (green) network in non-glycated and glycated matrix. Scale bar = 100 μm (g) Immunofluorescence staining images against YAP (red) in non-glycated and glycated matrix. Nucleus (blue) were counter-stained by DAPI. Scale bars=50 μm (h) Cytoplasmic and nuclear YAP protein expression in non-glycated and glycated matrix. Loading controls of cytoplasmic and nuclear proteins are β-tubulin and Lamin A/C, respectively. (For interpretation of the references to colour in this figure legend, the reader is referred to the web version of this article.)

We found that 444 genes were significantly up-regulated in CAF (FC[CAF/NF]>1, $p<0.05$), and those genes were strongly associated with the AGE–RAGE signaling pathway (KEGG: hsa04933) (Fig. 2b). The Gene Ontology results indicate that AGE–RAGE signaling leads to CAF activation in the tumor microenvironment.

In addition to the contribution of RAGE-dependent signaling, we postulated that integrins are activated by mechanical stimuli from within the AGE-modified ECM. The formation of AGEs on ECM molecules alters the structure of the matrix and increases stiffness. Once integrin-based adhesions form, activated integrins can facilitate the focal adhesion (FA)-mediated signaling pathway; Rho A and ROCK1/2 then generate myosin-mediated contractile force and promote YAP nuclear translocation as transcriptional regulators [27].

We selected six genes related to either the AGE–RAGE interaction (AGER) or integrin-mediated mechanotransduction (ITGB1, PTK2, RHOA, and ROCK1/2) to assess protein and mRNA expression in response to matrix glycation (Fig. 2c, d). In the glycated matrix, RAGE mRNA and protein expression were up-regulated (Fig. 2c, d). The five mechano-responsive genes (ITGB1, PTK2, RHOA, and ROCK1/2) were also significantly up-regulated in the glycated matrix (Fig. 2c). Similarly, the protein expression levels of Integrin $\beta 1$ and pFAK^{Y397} were increased in the glycated matrix (Fig. 2d). These results indicate that AGE-mediated matrix remodeling stimulates both the activation of RAGE and integrin-mediated mechanotransduction signaling.

Furthermore, to clarify the standalone effect of AGE on YAP expression, we introduced the AGE-BSA solution to the non-glycated matrix. Although the AGEs treatment conditions were different between pre-glycated matrix (as a crosslinked form, 500 mM of D-ribose in 10 mg/ml collagen solution) and AGE-BSA solution (as a soluble form, 250 mM of D-ribose in 5 mg/ml BSA solution), AGE-BSA solution was sufficient enough to confirm the standalone effect of AGE. The addition of AGE-BSA solution up-regulated RAGE and YAP expression in the non-glycated collagen matrix, but there was no change in integrin ß1 protein expression (Supplementary Fig. S2a). We observed nuclear YAP in the AGE-treated condition (Supplementary Fig. S2b, c). Furthermore, cell proliferation significantly increased by treating AGE (Supplementary Fig. S2d). Based on these results, we found that the standalone effect of AGE may regulate RAGE and YAP expression, independent of the mechanotransduction signaling pathway.

3.3. Matrix glycation induces CAF-like phenotypic changes in cultured fibroblasts

To elucidate the effects of matrix glycation on fibroblast activation, we first performed cell proliferation analyses using the WST-8 assay to quantify one of the main features of fibroblast activation: enhanced proliferation [28]. The proliferation rates of fibroblasts on days 4 and 7 were significantly increased in the glycated matrix compared to those of the non-glycated matrix (Fig. 3a). Further, the fibroblasts in the non-glycated matrix were spindle-shaped, whereas the fibroblasts in the glycated matrix were stellate with curved actin cytoskeletons (Fig. 3b).

Next, we analyzed the mRNA and protein expression of fibroblast activation markers, including alpha-smooth muscle actin (α-SMA), fibroblast activation protein (FAP), vimentin, and fibronectin

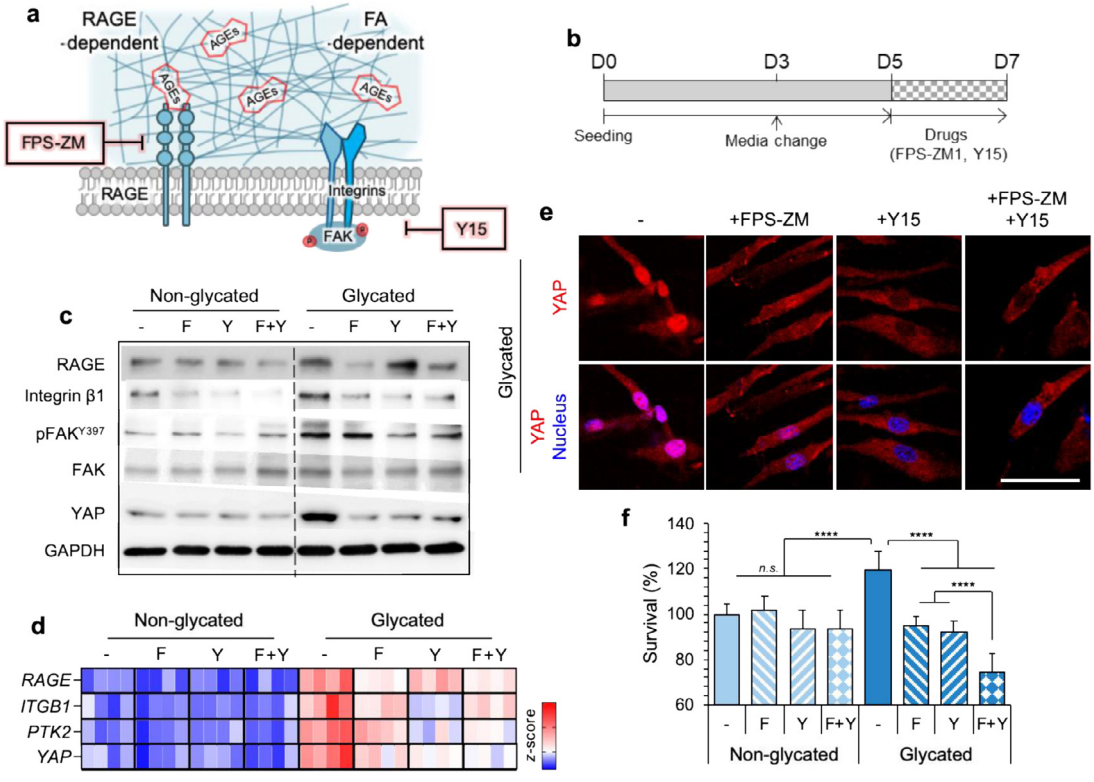

Fig. 4. Effect of RAGE inhibition on CAF-like phenotype through mechanotransduction signaling. (a) Schematics of RAGE- and FA-dependent signaling pathways in the glycated matrix. FPS-ZM1 (specific RAGE inhibitor) and Y15 (inhibitor of FAK phosphorylation) were used to inhibit RAGE and FA signaling. (b) Timeline of drugs treatment. (c) RAGE, Integrin ß1, pFAK, FAK, and YAP protein expression depending on drug treatment conditions in non-glycated and glycated matrix. Loading control is GAPDH. (d) Heatmap represented RAGE, ITGB1, PTK2, and YAP1 mRNA expression depending on drug treatment conditions in non-glycated and glycated matrix. Relative mRNA expression was normalized by GAPDH, and represented by z-score. (e) Immunofluorescence staining of YAP (red) depending on drug treatment conditions in glycated matrix. Nucleus were counterstained by DAPI (blue). Scale bar = 50 μm (f) Effect of drugs on fibroblast viability in non-glycated and glycated collagen matrix depending on drug treatment conditions. Significance; ****; $p<0.0001$, n.s.: no significance. (For interpretation of the references to colour in this figure legend, the reader is referred to the web version of this article.)

[15,28–30]. The expression of α-SMA (ACTA2), FAP (FAP), and vimentin (VIM) mRNA was significantly upregulated in fibroblasts cultured in the glycated matrix compared with those cultured in the non-glycated condition (Fig. 3c). The α-SMA and FAP protein levels were also strikingly increased in the glycated matrix (Fig. 3d, e). Notably, the glycated matrix-stimulated fibroblasts secreted significantly more fibronectin than those in the non-glycated matrix (Fig. 3f).

In addition to examining well-known fibroblast activation markers, we examined Yes-associated proteins (YAP) expression. YAP is pre-dominantly observed in the cytoplasm in normal fibroblasts, but it is localized in the nucleus in CAFs in response to a stiff matrix [31]. Through immunostaining, we observed noticeably higher amounts of nuclear YAP in fibroblasts in the glycated matrix, while mostly cytoplasmic YAP was observed in the non-glycated matrix (Fig. 3g). Higher nuclear YAP localization in glycated matrices was confirmed through western blotting (Fig. 3h), indicating that YAP activation also occurs in response to mechanotransduction resulting from increased stiffness of the AGE-modified matrix.

Our results confirmed that glycated matrices alter fibroblasts to a CAF-like phenotype, suggesting that fibroblast activation in the AGE-modified matrix could be inhibited by modulating either RAGE or mechanotransduction signaling pathways.

3.4. Targeting RAGE and mechanotransduction signaling to inhibit CAF-like phenotypic changes

To determine whether the inhibition of mechanotransduction signaling synergizes with RAGE inhibition in AGE-modified matrix-stimulated fibroblasts, we treated the cells with inhibitors of the major signaling transduction pathways. RAGE function was inhibited with FPS-ZM1, a high-affinity RAGE-specific inhibitor/blocker (Ki = 25 nM) [32,33], and the effect of FAs on mechanotransduction was blocked with Y15, a small molecule inhibitor of phos-

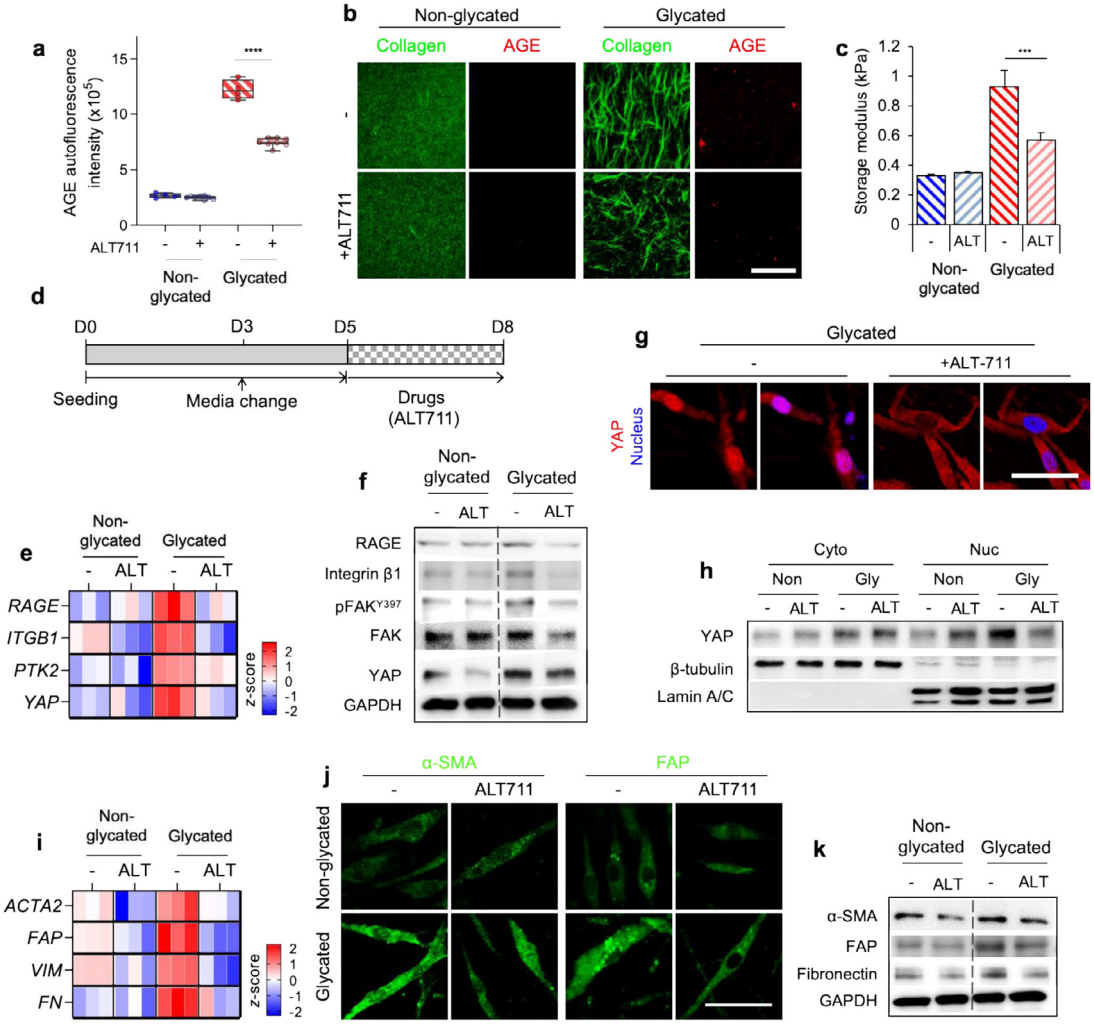

Fig. 5. AGE-targeting matrix modulation to inhibit CAF-like transition. (a) AGE-autofluorescence intensity by treating ALT-711 (AGE-crosslinking breaker) for 3 days in non-glycated and glycated collagen matrix. ****;$p<0.0001$ (b) Immunostaining images of glycated collagen shows that AGE observed by treating ALT-711 compared to non-treated condition. Green: collagen fiber stained by Col-F, red: AGEs. Scale bar = 50 μm (c) The storage modulus after ALT-711 treatment for 3 days in non-glycated and glycated collagen matrix. ***;$p<0.001$ (d) Overall timeline of ALT-711 treatment during fibroblast culture. (e) Heatmap represented the relative mRNA expression of RAGE, ITGB1, PTK2 and YAP1 in non-glycated and glycated matrix. Gene expression normalized by GAPDH. Expression represented by z-score. (f) RAGE, Integrin ß1, pFAK, FAK and YAP protein expression with ALT-711 in non-glycated and glycated matrix. Loading control is GAPDH. (g) Immunofluorescence staining of YAP (red) with ALT-711 in non-glycated and glycated matrix. Nucleus were counterstained by DAPI (blue). Scale bar = 50 µm (h) Cytoplasmic and nuclear YAP protein expression in non-glycated and glycated matrix with ALT-711. Loading controls of cytoplasmic and nuclear proteins are β-tubulin and Lamin A/C, respectively. (i) Heatmap represented the relative mRNA expression of ACTA2, FAP, VIM and FN in non-glycated and glycated matrix. Gene expression normalized by GAPDH. Expression represented by z-score. (j) Immunofluorescence staining of α-SMA and FAP (green) with ALT-711 in non-glycated and glycated matrix. Scale bar = 50 µm (k) α-SMA, FAP, and fibronectin protein expression with ALT-711 in non-glycated and glycated matrix. Loading control is GAPDH. (For interpretation of the references to colour in this figure legend, the reader is referred to the web version of this article.)

phorylation at the Y397 site of FAK (PTK2) [34] (Fig. 4a). After 5 days of culture in glycated and non-glycated matrices, cells were treated with drugs for 2 days in four experimental groups: no drug treatment (–), FPS-ZM1 treatment (F, 1 μM), Y15 treatment (Y, 5 μM), and combined treatment of FPS-ZM1 and Y15 ($F + Y$) (Fig. 4b). The FPS-ZM1-only treatment significantly suppressed RAGE expression at the AGER mRNA and protein levels, but there was no change in PTK2 mRNA or pFAK protein expression. In contrast, the Y15-only treatment inhibited FAK phosphorylation, but not RAGE expression (Fig. 4c). This indicated that each inhibitor blocked its respective pathway separately without interfering with the other. Co-treatment ($F + Y$) inhibited both RAGE and pFAK expression of AGER and PTK2 mRNA and protein (Fig. 4c, d). The effects of co-treatment were more pronounced in the glycated matrix, where the cells over-expressed RAGE and pFAK. Note that nuclear YAP returns to the cytoplasm in the glycated matrix in the Y-only and $F + Y$ co-treatment (Fig. 4e). This indicated that FA inhibition strictly affected YAP activation in fibroblasts. In the non-glycated matrix, cytoplasmic YAP was observed regardless of the treatment (Supplementary Figure S3a). Furthermore, cell proliferation was significantly suppressed in the glycated matrix with co-treatment when compared to standalone drug treatments (Fig. 4f). The mRNA expressions of ACTA2, FAP, VIM, and FN mRNA also decreased substantially by ~1.4, 2.4, 1.3, and 1.7-fold, respectively, in the glycated matrix with the dual treatment ($F + Y$), but not in the non-glycated matrix (Supplementary Figure S3b). The expressions of α-SMA and FAP also strikingly decreased with the three drug treatments (Supplementary Figure S3c). However, we found no significant difference among the drug treatment conditions in terms of the expression of fibroblast markers.

To clarify the role of RAGE on YAP expression, we constructed shRNA-mediated RAGE-depleted hTERT NOF cells. The shRAGE suppressed RAGE and YAP expression, but there was no change in integrinß1 protein expression (Supplemented Fig. S4a). Also, nuclear YAP was observed in the glycated matrix in wild type, but not in RAGE-depleted cells (Supplemented Fig. S4b, c). Furthermore, cell proliferation was significantly suppressed in RAGE-depleted cells (Supplemented Fig. S4d). Based on these results, we found that RAGE regulate YAP expression, independent to mechanotransduction signaling pathway.

Based on these results, we suggest that intracellular targeting via the inhibition of either the RAGE-dependent or mechanotransduction-dependent signaling pathway could neutralize the effects of accumulated AGEs within the matrix and lead to decreased fibroblast activation.

3.5. Effect of AGE-breaker on the CAF-like transition

In addition to intracellular targeting, we examined whether the removal of irreversibly bound AGEs within the matrix regulated fibroblast activation directly by eliminating both the AGE–RAGE interaction and mechanotransduction. To do this, we used the AGE-breaker ALT-711 (4,5-dimethyl-3-phenacylthiazolium chloride or alagebrium) [35,36]. First, we examined whether there were any physical differences in collagen matrices upon addition of ALT-711. After a 3-day treatment, AGE autofluorescence was decreased 1.6-fold in the glycated matrix, but not in the non-glycated matrix (Fig. 5a). After ALT 711 treatment, the thick, linearized collagen fibers in the glycated matrix appeared fragmented and AGE fluorescence decreased (collagen, green; AGE, red; Fig. 5b). Consequently, bulk storage modulus was decreased ~1.64-fold in the glycated matrix due to AGE disintegration ($p<0.001$, Fig. 5c).

To analyze the effects of breaking AGE on fibroblast activation, fibroblasts in glycated and non-glycated matrices were treated with ALT-711 for 3 days after a 5-day normal culture period (Fig. 5d). The ALT-711 treatment significantly attenuated mechanotransduction signaling, including integrin β1, FAK mRNA expression, and RAGE expression (Fig. 5e). Adding ALT-711 to the glycated matrix noticeably decreased pFAK (Fig. 5f). Furthermore, the total YAP mRNA and protein expression in glycated matrix were significantly reduced with the ALT-711 treatment (Fig. 5e, f). Interestingly, nuclear YAP expression was significantly decreased in the glycated matrix, and it was relocated to the cytoplasm with ALT-711 treatment (Fig. 5g, h). We also confirmed that ALT-711 treatment reduced the expression of α-SMA (ACTA2), FAP (FAP), fibronectin (FN), and vimentin (VIM) mRNA and protein in the glycated matrix (Fig. 5i–k). Furthermore, cell viability was significantly suppressed in glycated matrix with ALT-711 treatment (Supplementary Fig S5). Also, decreased both AGE-RAGE and mechanotransduction signaling by treating ALT-711 regulated ROS production (Supplementary Fig. S6). These results suggest that the direct breakup of accumulated AGE within the matrix has dual targets for CAF-like phenotype transition in response to glycated matrix.

4. Conclusion

In summary, we demonstrated that AGE-mediated matrix remodeling activates fibroblasts via biochemical and biomechanical changes in the ECM. Matrix glycation is crucial for inducing the activation of quiescent fibroblasts in the hyperglycemic tumorigenic stroma. Accumulated AGE within the matrix induces a CAF-like phenotype transition of fibroblasts via the AGE–RAGE interaction and integrin-mediated mechanotransduction. In response to the stiffened matrix, fibroblasts overexpress mechano-sensitive genes, promoting YAP nuclear location. We found that targeting either the AGE–RAGE or integrin-mediated mechanotransduction pathways attenuates fibroblast activation. Moreover, we suggest that extracellular targeting using an AGE-breaker can attenuate CAF-like transitions, which may have clinical potential in numerous diseases that accompany glycation-mediated, extracellular matrix remodeling.

5. Author contributions

M. Jang, Y. Lee and P. Kim designed the experiments. M. Jang, S. W. Oh, Y. Lee, J. Y. Kim, E. S. Ji performed experiments and analyzed the data. M. Jang, S.W. Oh, and P. Kim wrote the manuscript, and all authors discussed the results and reviewed the manuscript.

Declaration of Competing Interest

The authors declare no competing financial interest.

The authors declare that they have no known competing financial interests or personal relationships that could have appeared to influence the work reported in this paper.

Acknowledgments

This research was supported by Basic Science Research Program through the National Research Foundation of Korea (NRF) funded by the Ministry of Education (NRF- 2019R1A2C2084142) and Korea Health Technology R&D Project through the Korea Health Industry Development Institute (KHIDI) funded by the Ministry of Health & Welfare, Republic of Korea [HI14C1324]. This research was also supported by a grant from the Korea Basic Science Institute (KBSI) (Research Grant No. C060100). This work was supported by Research Program of the National Research Foundation (NRF) funded by the Ministry of Science & ICT (NRF-2021M3H9A2097108).

Supplementary materials

Supplementary material associated with this article can be found, in the online version, at doi:10.1016/j.actbio.2022.01.040.

References

[1] P. Lu, V.M. Weaver, Z. Werb, The extracellular matrix: a dynamic niche in cancer progression, J. Cell Biol. 196 (4) (2012) 395–406.
[2] C.C. DuFort, M.J. Paszek, V.M. Weaver, Balancing forces: architectural control of mechanotransduction, Nat. Rev. Mol. Cell Biol. 12 (5) (2011) 308–319.
[3] V. Vicens-Zygmunt, S. Estany, A. Colom, A. Montes-Worboys, C. Machahua, A.J. Sanabria, R. Llatjos, I. Escobar, F. Manresa, J. Dorca, D. Navajas, J. Alcaraz, M. Molina-Molina, Fibroblast viability and phenotypic changes within glycated stiffened three-dimensional collagen matrices, Respir. Res. 16 (2015) 82.
[4] H. Dandia, K. Makkad, P. Tayalia, Glycated collagen - a 3D matrix system to study pathological cell behavior, Biomater. Sci. 7 (8) (2019) 3480–3488.
[5] H.E. Barker, J. Chang, T.R. Cox, G. Lang, D. Bird, M. Nicolau, H.R. Evans, A. Gartland, J.T. Erler, LOXL2-mediated matrix remodeling in metastasis and mammary gland involution, Cancer Res. 71 (5) (2011) 1561–1572.
[6] K.R. Levental, H. Yu, L. Kass, J.N. Lakins, M. Egeblad, J.T. Erler, S.F. Fong, K. Csiszar, A. Giaccia, W. Weninger, M. Yamauchi, D.L. Gasser, V.M. Weaver, Matrix crosslinking forces tumor progression by enhancing integrin signaling, Cell 139 (5) (2009) 891–906.
[7] P. Stattin, O. Bjor, P. Ferrari, A. Lukanova, P. Lenner, B. Lindahl, G. Hallmans, R. Kaaks, Prospective study of hyperglycemia and cancer risk, Diabetes Care 30 (3) (2007) 561–567.
[8] D.P. Turner, Advanced glycation end-products: a biological consequence of lifestyle contributing to cancer disparity, Cancer Res. 75 (10) (2015) 1925–1929.
[9] C. Ott, K. Jacobs, E. Haucke, A. Navarrete Santos, T. Grune, A. Simm, Role of advanced glycation end products in cellular signaling, Redox. Biol. 2 (2014) 411–429.
[10] M.W. Conklin, J.C. Eickhoff, K.M. Riching, C.A. Pehlke, K.W. Eliceiri, P.P. Provenzano, A. Friedl, P.J. Keely, Aligned collagen is a prognostic signature for survival in human breast carcinoma, Am. J. Pathol. 178 (3) (2011) 1221–1232.
[11] R. Malik, P.I. Lelkes, E. Cukierman, Biomechanical and biochemical remodeling of stromal extracellular matrix in cancer, Trends Biotechnol. 33 (4) (2015) 230–236.
[12] P. Schedin, P.J. Keely, Mammary gland ECM remodeling, stiffness, and mechanosignaling in normal development and tumor progression, Cold Spring Harb. Perspect. Biol. 3 (1) (2011) a003228.
[13] D.L. Matera, W.Y. Wang, M.R. Smith, A. Shikanov, B.M. Baker, Fiber density modulates cell spreading in 3D interstitial matrix mimetics, ACS Biomater. Sci. Eng. 5 (6) (2019) 2965–2975.
[14] V. Petrova, M. Annicchiarico-Petruzzelli, G. Melino, I. Amelio, The hypoxic tumour microenvironment, Oncogenesis 7 (1) (2018) 10.
[15] K.C. Valkenburg, A.E. de Groot, K.J. Pienta, Targeting the tumour stroma to improve cancer therapy, Nat. Rev. Clin. Oncol. 15 (6) (2018) 366–381.
[16] M. Kalli, P. Papageorgis, V. Gkretsi, T. Stylianopoulos, Solid stress facilitates fibroblasts activation to promote pancreatic cancer cell migration, Ann. Biomed. Eng. 46 (5) (2018) 657–669.
[17] F.M. Watt, W.T. Huck, Role of the extracellular matrix in regulating stem cell fate, Nat. Rev. Mol. Cell Biol. 14 (8) (2013) 467–473.
[18] I. Jang, K.A. Beningo, Integrins, CAFs and mechanical forces in the progression of cancer, Cancers (Basel) 11 (5) (2019).
[19] S.R. Caliari, M. Perepelyuk, B.D. Cosgrove, S.J. Tsai, G.Y. Lee, R.L. Mauck, R.G. Wells, J.A. Burdick, Stiffening hydrogels for investigating the dynamics of hepatic stellate cell mechanotransduction during myofibroblast activation, Sci. Rep. 6 (2016) 21387.
[20] J.M. Lee, S.P. Veres, Advanced glycation end-product cross-linking inhibits biomechanical plasticity and characteristic failure morphology of native tendon, J. Appl. Physiol. 126 (4) (1985) 832–841 2019.
[21] J.A. Lin, C.H. Wu, G.C. Yen, Perspective of advanced glycation end products on human health, J. Agr. Food Chem. 66 (9) (2018) 2065–2070.
[22] M.S. Hall, F. Alisafaei, E. Ban, X.Z. Feng, C.Y. Hui, V.B. Shenoy, M.M. Wu, Fibrous nonlinear elasticity enables positive mechanical feedback between cells and ECMs, P. Natl. Acad. Sci. USA 113 (49) (2016) 14043–14048.
[23] L. Robert, J. Labat-Robert, Role of the Maillard reaction in aging and age-related diseases. studies at the cellular-molecular level, Clin. Chem. Lab. Med. 52 (1) (2014) 5–10.
[24] T.A. Collier, A. Nash, H.L. Birch, N.H. de Leeuw, Effect on the mechanical properties of type I collagen of intra-molecular lysine-arginine derived advanced glycation end-product cross-linking, J. Biomech. 67 (2018) 55–61.
[25] M.C. Lampi, C.A. Reinhart-King, Targeting extracellular matrix stiffness to attenuate disease: from molecular mechanisms to clinical trials, Sci. Transl. Med. 10 (422) (2018).
[26] Z.Q. Sun, S.S. Guo, R. Fassler, Integrin-mediated mechanotransduction, J. Cell Biol. 215 (4) (2016) 445–456.
[27] G. Nardone, J. Oliver-De La Cruz, J. Vrbsky, C. Martini, J. Pribyl, P. Skladal, M. Pesl, G. Caluori, S. Pagliari, F. Martino, Z. Maceckova, M. Hajduch, A. Sanz-Garcia, N.M. Pugno, G.B. Stokin, G. Forte, YAP regulates cell mechanics by controlling focal adhesion assembly, Nat. Commun. 8 (2017) 15321.
[28] L.V. Ireland, A. Mielgo, Macrophages and fibroblasts, key players in cancer chemoresistance, Front. Cell Dev. Biol. 6 (2018).
[29] Y. Fuyuhiro, M. Yashiro, S. Noda, S. Kashiwagi, J. Matsuoka, Y. Doi, Y. Kato, T. Hasegawa, T. Sawada, K. Hirakawa, Upregulation of cancer-associated myofibroblasts by TGF-beta from scirrhous gastric carcinoma cells, Brit. J. Cancer 105 (7) (2011) 996–1001.
[30] R. Kalluri, The biology and function of fibroblasts in cancer, Nat. Rev. Cancer 16 (9) (2016) 582–598.
[31] F. Calvo, N. Ege, A. Grande-Garcia, S. Hooper, R.P. Jenkins, S.I. Chaudhry, K. Harrington, P. Williamson, E. Moeendarbary, G. Charras, E. Sahai, Mechanotransduction and YAP-dependent matrix remodelling is required for the generation and maintenance of cancer-associated fibroblasts, Nat. Cell Biol. 15 (6) (2013) 637 -+.
[32] H. Lee, H.R. Heo, J.Y. Kim, W.J. Kim, S.H. Hong, S.R. Yang, FPS-ZM1-induced blocking of RAGE alleviates elastase-induced emphysema development by preventing RAGE-DAMP-Nrf2 signaling, Eur. Respir. J. 50 (2017).
[33] R. Deane, I. Singh, A.P. Sagare, R.D. Bell, N.T. Ross, B. LaRue, R. Love, S. Perry, N. Paquette, R.J. Deane, M. Thiyagarajan, T. Zarcone, G. Fritz, A.E. Friedman, B.L. Miller, B.V. Zlokovic, A multimodal RAGE-specific inhibitor reduces amyloid beta-mediated brain disorder in a mouse model of Alzheimer disease, J. Clin. Invest. 122 (4) (2012) 1377–1392.
[34] M. Jang, I. Koh, J.E. Lee, J.Y. Lim, J.H. Cheong, P. Kim, Increased extracellular matrix density disrupts E-cadherin/beta-catenin complex in gastric cancer cells, Biomater. Sci. 6 (10) (2018) 2704–2713.
[35] D.A. Kass, Getting better without AGE - new insights into the diabetic heart, Circ. Res. 92 (7) (2003) 704–706.
[36] M.L. Freidja, K. Tarhouni, B. Toutain, C. Fassot, L. Loufrani, D. Henrion, The AGE-breaker ALT-711 restores high blood flow-dependent remodeling in mesenteric resistance arteries in a rat model of type 2 diabetes, Diabetes 61 (6) (2012) 1562–1572.